Preprint, published in Shock Waves 25(3), 217-219, 2015
https://doi.org/10.1007/s00193-014-0509-4

Shock Waves
DOI 10.1007/s00193-014-0509-4

ORIGINAL ARTICLE

Ignition delay-time behind reflected shock waves of small hydrocarbons–nitrous oxide(–oxygen) mixtures

R. Mével · J. E. Shepherd

Received: 31 October 2013 / Revised: 19 April 2014 / Accepted: 23 April 2014

Abstract Although nitrous oxide has been identified as an important intermediate during the combustion of many solid propellants, there is a limited amount of data concerning the high-temperature oxidation of hydrocarbons by nitrous oxide. In the present study, ignition delay-times of small hydrocarbon–N_2O mixtures with and without O_2 were investigated through shock-tube experiments and chemical kinetic simulations. Experimentally, it is shown that the addition of oxygen induces a significant reduction of the activation energy of the ignition process. Simulations demonstrate that delay-times are usually satisfactorilly predicted but that the detailed reaction models used do not capture all the features of the OH* emission profiles.

Keywords Small hydrocarbons · Reflected shock wave · Ignition delay-time · Kinetic modeling

1 Introduction

Numerous propellants and energetic materials are characterized by chemical structures with one or several nitro and/or nitrate groups [1]. Their combustion is a complex process which involves physico-chemical phenomena occurring both in the solid and the gas phases as well as at their interface [1,2]. Nitro- and nitrate-based compounds are also attractive as auto-ignition promoters in diesel engines [3]. In addition to numerous practical propulsion applications, the chemistry of nitrogen dioxide is relevant to the combustion of a number of mixtures such as $CH_3NO_2(–O_2)$, $H_2–NO_2/N_2O_4$, $CH_4–NO_2/N_2O_4$ and $C_2H_6–NO_2/N_2O_4$ which exhibit a double cellular structure when detonating [4–6] and multiple zone flame structures [7–9]. Nitrous oxide has been identified as an important intermediate during the combustion of many solid propellants [10,11]. Consequently, it is important to properly describe the chemistry of hydrocarbon oxidation with N_2O to accurately model the gas phase kinetics of solid propellant combustion. However, there is a limited amount of data in the high-temperature regime.

The purposes of the present study are to experimentally measure the auto-ignition delay-time of some small hydrocarbon (CH_4, C_2H_6, C_2H_4, C_2H_2)–nitrous oxide mixtures with and without oxygen using the shock-tube technique and to test the validity of several detailed reaction models.

2 Materials and methods

2.1 Materials

The experimental setup used in the present study is the GALCIT six-inch shock tube. It is composed of three parts separated by two diaphragms. The driver section and the driven section are 6.19 and 11.28 m long, respectively, with a 15.24 cm inner diameter. The test section is 2.44 m long and has a 7.62 cm inner diameter. A 2.03 long, 7.62 cm inner diameter "cookie-cutter" is used to propagate the shock wave from the driven to the test section. The cookie-cutter eliminates the incident shock wave diffraction at the transition from the shock tube to the test section. The sharpened edge of the cookie-cutter enables a smooth cut-out of the central part of the incident shock wave generated in the shock tube. Its length was chosen to maximize the observation time. The test section is equipped with 3 pressure transducers and a photo-

Communicated by G. Ciccarelli.

R. Mével (✉) · J. E. Shepherd
Graduate Aeronautical Laboratories, California Institute of Technology, Pasadena, USA
e-mail: mevel@caltech.edu

Published online: 14 May 2014

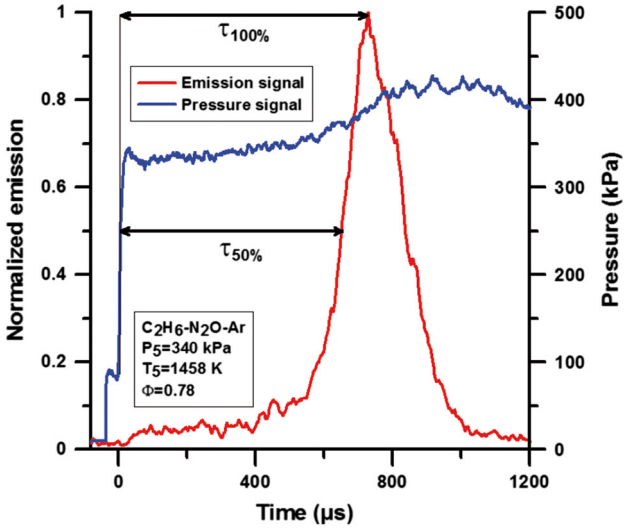

Fig. 1 Typical experimental signals and definitions of the two characteristic times of reaction

multiplier tube mounted in front of a quartz window located 13 mm from the end wall. The uncertainty on the incident shock wave velocity measurement is <2 %. An optical fiber was employed to collect the light emission from the reacting mixture and a narrow passband filter centered around 307 nm was used to select the emission originating from the ($A^2\Sigma^+$–$X^2\Pi$) OH radical electronic transition. The ignition was studied behind reflected shock waves using two characteristic times of reaction: the times to half, $\tau_{50\%}$, and to the maximum, $\tau_{100\%}$, of the emission peak. The uncertainty on this parameter is estimated to be on the order of 20 % [12]. Figure 1 shows typical experimental signals and illustrates the definition of the two characteristic times of reaction used.

All gases were of research grade and were obtained from Air Liquide. Gaseous mixtures were prepared in a 9.25 L mixture vessel, using the partial pressure method, and were mixed with a brushless fan mounted inside the vessel. The residual pressures in the mixture vessel and the test section were below 1 Pa. The argon dilution was 96 %. Table 1 summarizes the mixture compositions and experimental conditions. The equivalence ratio was defined in terms of atom mole fractions X_i as:

$$\Phi = \frac{2 \cdot X_C + 0.5 \cdot X_H}{X_O}, \quad (1)$$

where X_C, X_H, and X_O refer to the C, H and O element, respectively.

2.2 Modeling

Four reaction mechanisms have been evaluated with respect to the present experimental results: (i) the mechanism of Konnov [13], 1,200 reactions and 127 species, (ii) the mechanism of Dagaut [14], 925 reactions and 128 species, (iii) the GRI-Mech 3.0 [15], 325 reactions and 53 species, and (iv) the Blanquart mechanism [11,14,16–20], 853 reactions and 110 species. In each case, the thermodynamic data supplied with each model were used. A sub-mechanism for the kinetics of excited OH radicals, OH*, from Hall and Petersen studies [21,22], has been added in each model. The concentration of OH* is typically 6 orders of magnitude lower than that of OH radicals so that no significant modifications of the ground-state chemistry are expected by the inclusion of OH* chemical pathways. However, a number of studies [17,23–26] have demonstrated that the chemical pathways forming OH* radicals differ from those forming the ground-state OH radical, so that it is required to include a sub-mechanism for their chemistry when modeling ignition delay-times obtained from OH* emission. Modeling of the experimental results used the Senkin code [27] of the Chemkin II package [28]. Several reactor models, namely constant volume, CV, constant pressure, CP, and time-dependent volume reactor, VTIM [29], have been employed. The delay-time was calculated for every

Table 1 Mixture compositions and experimental conditions examined in the present study

No.	Φ	X_{CH_4}	$X_{C_2H_6}$	$X_{C_2H_4}$	$X_{C_2H_2}$	X_{O_2}	X_{N_2O}	T_5 (K)	P_5 (kPa)
1	1.11	0.00867	–	–	–	–	0.03133	1,527–1,925	222–320
2	0.93	0.01066	–	–	–	0.01666	0.01266	1,478–1,945	249–321
3	0.78	–	0.00400	–	–	–	0.03598	1,398–1,730	282–359
4	1.12	–	0.00799	–	–	0.01798	0.01398	1,272–1,641	295–397
5	1.80	0.00532	0.00466	–	–	–	0.02994	1,506–1,862	241–334
6	1.11	0.00533	0.00466	–	–	0.01865	0.01133	1,312–1,693	279–361
7	1.37	–	–	0.00733	–	–	0.03200	1,399–1,773	254–348
8	1.41	–	–	0.01067	–	0.01600	0.01333	1,269–1,620	291–387
9	0.80	–	–	–	0.00549	–	0.03447	1,436–1,708	291–346
10	1.23	–	–	–	0.01000	0.01000	0.02050	1,311–1,545	330–378

In all cases, the balance of the composition is Ar

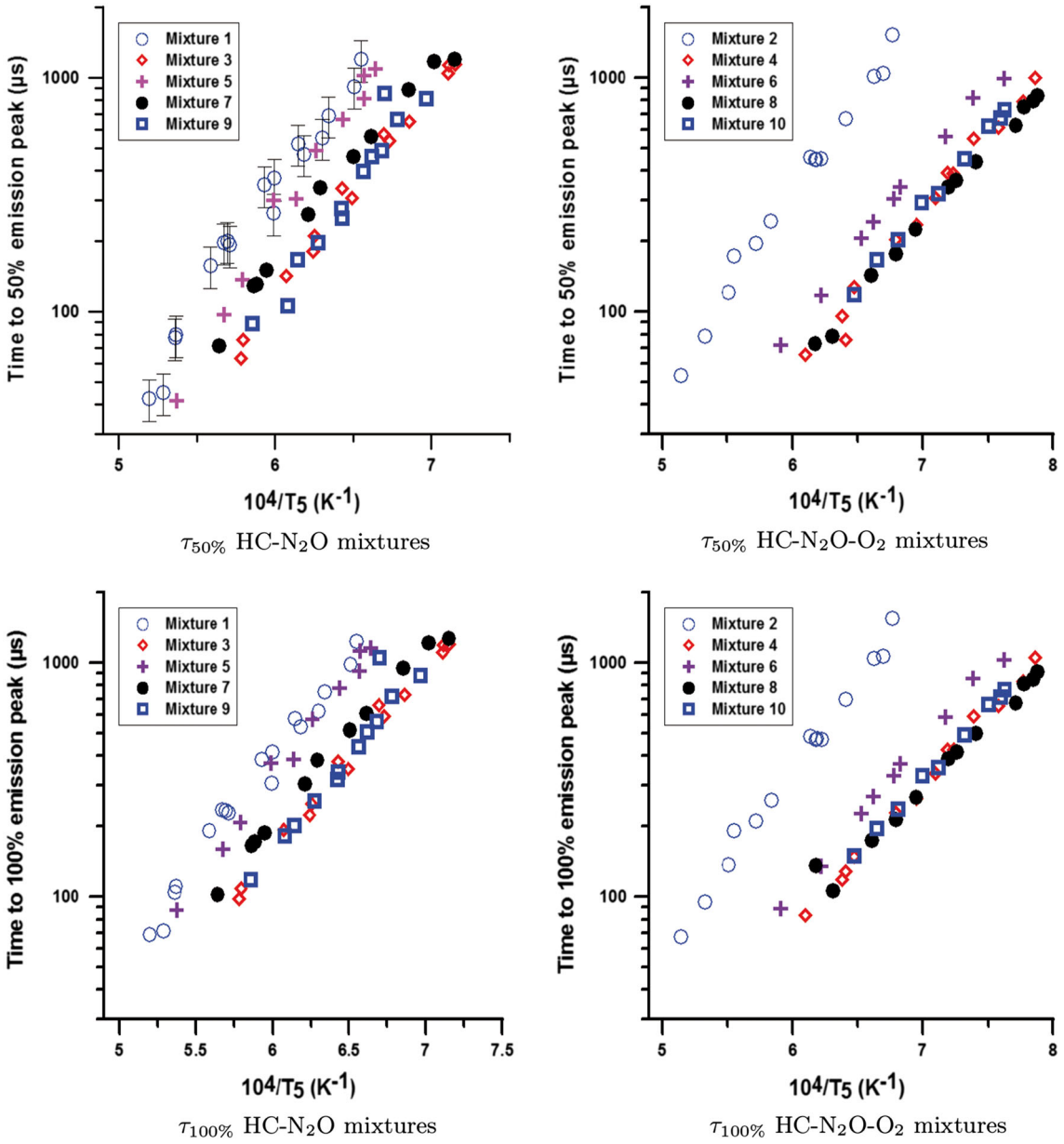

Fig. 2 Experimental ignition delay-time of small hydrocarbon–N_2O(–O_2) mixtures

data point using the reflected temperature and pressure computed from the measured shock speed and initial conditions for each case. Analyses of the reaction pathways, sensitivity coefficients, and energy release rate have also been performed using Senkin.

3 Results and discussion

3.1 Experimental results

Ignition delay-time of small hydrocarbon–N_2O mixtures with and without O_2 was measured behind a reflected shock wave in the temperature and pressure ranges 1,269–1,945 K and 222–397 kPa, respectively. Figure 2 presents the data obtained for the 10 mixtures studied. Mixtures containing methane exhibit significantly longer ignition delay-times, up to 30 % longer for mixtures with both CH_4 and C_2H_6, and up to 5 times longer for mixtures with only CH_4. Table 2 summarizes the pre-exponential factors and activation energies obtained by least-squares fitting the experimental data for each mixture. Mixtures with both O_2 and N_2O demonstrate significantly lower activation energies, 25 % lower on average, compared to mixtures with N_2O as the only oxidant. This observation is consistent with previous results obtained with H_2–O_2–(N_2O)–Ar mixtures [26].

Table 2 Arrhenius-like parameters for the different mixtures studied

Mixture	$\tau_{50\%}$		$\tau_{100\%}$	
	A	E_a	A	E_a
1	$3.40E^{-4}$	191	$2.03E^{-3}$	168
2	$3.23E^{-3}$	159	$6.91E^{-3}$	150
3	$5.80E^{-4}$	169	$3.07E^{-3}$	150
4	$3.93E^{-3}$	132	$1.41E^{-2}$	118
5	$6.25E^{-5}$	209	$1.59E^{-3}$	169
6	$1.23E^{-2}$	124	$3.22E^{-2}$	114
7	$1.85E^{-3}$	158	$7.33E^{-3}$	142
8	$9.46E^{-3}$	120	$5.12E^{-2}$	103
9	$2.41E^{-4}$	181	$2.13E^{-3}$	155
10	$5.72E^{-3}$	128	$1.66E^{-2}$	117

Pre-exponential factor, A, and activation energy, E_a, are expressed in μs and kJ/mol, respectively

For some of the mixtures studied, the OH* emission profiles demonstrated complex behavior with emission starting just after the reflected shock, levelling off and then rapidly increasing as the main exothermic oxidation step takes place. This phenomenon was found to be both mixture and temperature dependent. Such profiles were never observed for the mixtures with CH_4 as the only fuel. For the mixtures containing C_2H_6, the pre-ignition emission was always observed at intermediate and higher temperature, except for the C_2H_6–N_2O–O_2–Ar mixture for which this feature was not present. The amplitude of the first emission peak ranged from 5–10 % of the main peak at intermediate temperature to 30 % at high temperature. At the highest temperature studied, the two peaks merge and only one peak is seen. For the mixtures containing C_2H_2 and C_2H_4, the pre-ignition emission was visible only in the high-temperature range, irrespective of the presence or absence of oxygen. Figure 3 shows some typical examples of the observed emission profiles. Such complex emission features have also been reported by Rotavera et al. [30] during the oxidation of n-nonane by oxygen behind reflected shock wave.

3.2 Modeling results

3.2.1 Reactor model

In most shock-tube modeling studies, the homogeneous constant volume (CV) reactor model is used. Alternatively, a constant pressure (CP) process can be assumed under certain conditions. The effect of the reactor model employed on the modeling of the present data has been investigated using the Blanquart reaction mechanism. Figure 4 presents some typical results obtained for mixture 10, C_2H_2–N_2O–O_2–Ar. It is clearly seen that the predicted ignition delays are much longer in the case of the CP reactor. The mean error for the ten mixtures studied is around 22 % using a CV reactor model against 43 % if a CP reactor is assumed. The OH* profiles predicted with a CP reactor appear much broader than experimentally observed. Also, the relative amplitude of the pre-ignition emission peak is over-estimated. On the contrary, the CV reactor allows for a fair prediction of the emission peak shape.

Another type of reactor model which can be used to model auto-ignition delay-times obtained in shock tubes is the so-called VTIM reactor [29]. It consists in using a time-dependent volume based on the experimental pressure trace, assuming an isentropic process. The relevance of using such a reactor to model the data of the present study has been examined for mixture 2, CH_4–N_2O–O_2–Ar, which demonstrates the longest delay-times, and for mixture 7, C_2H_4–N_2O–Ar, which is among the most energetic mixtures studied. Figure 5 shows the results obtained with both reactor models. For mixture 2, the delays predicted with either reactor models are very close to each other. For mixture 7, larger differences are observed, especially at low temperature.

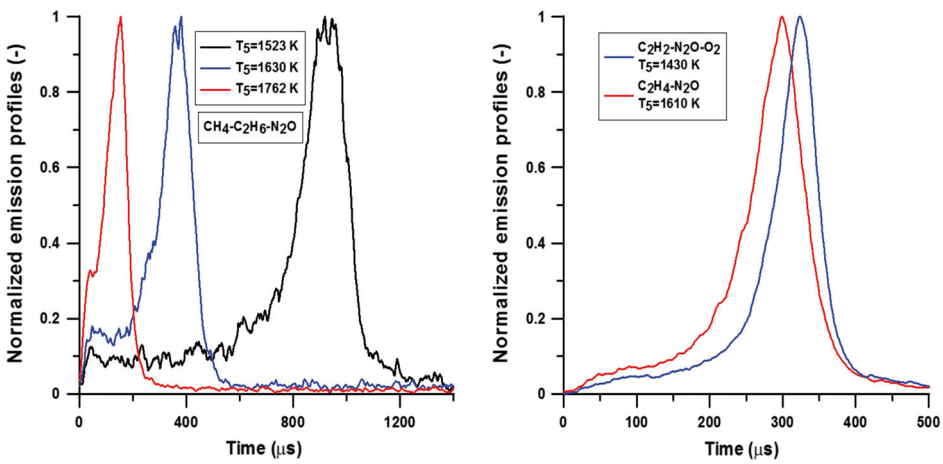

Fig. 3 Normalized experimental emission profiles of small hydrocarbon–N_2O(–O_2) mixtures

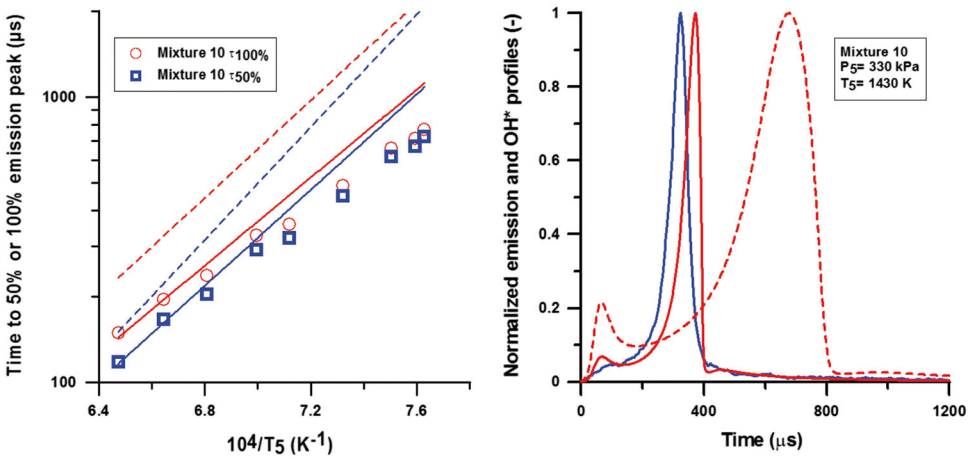

Fig. 4 Comparison between the prediction of the Blanquart reaction mechanism assuming either a CV reactor or a CP reactor. *Solid lines* CV reactor. *Dashed lines* CP reactor. The *blue* profile corresponds to the experimental emission profile

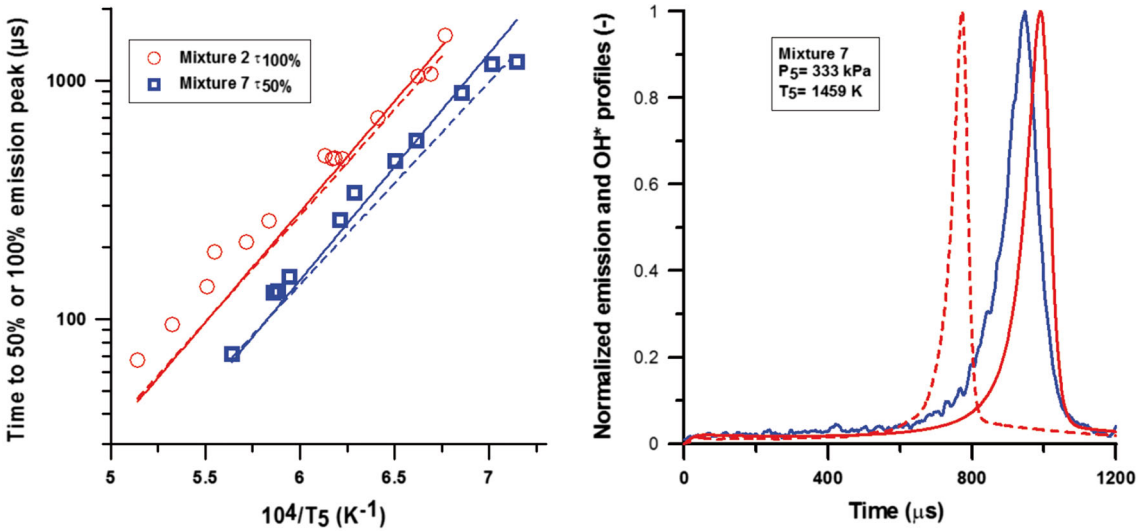

Fig. 5 Comparison between the prediction of the Caltech model assuming either a CV reactor or a VTIM reactor. *Solid lines* CV reactor. *Dashed lines* VTIM reactor. The *blue* profile corresponds to the experimental emission profile

On the average, a difference of 11 % is observed between the CV and VTIM delay-times, with the VTIM delays being shorter. Such a difference is within the experimental uncertainty. The mean error compared to the experimental values is 19 % for both reactor models. As shown in Fig. 5, the OH* profiles are essentially the same for both models and qualitatively similar to the experimental emission profile. For this particular condition, the profile obtained with the CV model is closest to the experimental one but the contrary applies for other conditions in the low-temperature range.

It is not clear whether the energy density or the composition of the mixture is responsible for the larger differences observed in the case of mixture 7. The nitrous oxide content in mixture 7 is much higher than in mixture 2, 3.2 vs. 1.3 % and N_2O favors mixture inhomogeneity behind reflected shock wave because it can result in shock wave bifurcation [31]. The extent of such a process in the present experiments is difficult to estimate and a two-step pressure jump typically seen when bifurcation occurs was not observed in our experiments. For some of the mixtures studied, in the low-temperature range, the VTIM reactor model is better than the CV model. A comprehensive study of the effect of the reactor model on the prediction of shock-tube experiments is beyond the scope of the present study. For most conditions studied, the CV model is a reasonable approximation and in the following sections of the paper, only the CV reactor model was used to perform the comparisons and analyses.

3.2.2 Reaction mechanism predictions

The reaction mechanisms of Konnov, Dagaut, Blanquart and the GRI-mech 3.0 were evaluated with respect to the present

Table 3 Relative error (%) for each of the reaction mechanisms used in the present study

Mixture	Konnov	GRI-3.0	Dagaut	Blanquart
1	15.6	18.1	16.1	22.6
2	21.7	17.2	16.8	20.2
3	12.1	35.1	68.6	15.1
4	19.1	26.6	37.3	31.2
5	11.7	30.2	48.4	13.2
6	16.0	15.5	73.7	20.0
7	13.4	25.1	72.7	17.7
8	12.8	87.3	48.2	43.2
9	22.7	65.9	34.0	12.4
10	60.7	73.2	70.7	24.4
Mean	19.5	37.9	45.9	22.1
Max	80.7	126.3	204.4	65.9
Min	0.9	0.1	0.6	0.1

data assuming the CV reactor model. The performance of the different reaction mechanisms was mainly evaluated using the mean error,

$$E_{\text{mean}} = \frac{1}{N}\sum_{i}^{N}\left|\frac{\Delta\tau}{\tau_{\text{expe}}}\right|, \tag{2}$$

where N is the number of data points, $\Delta\tau = \tau_{\text{model}} - \tau_{\text{expe}}$, with τ_{model} and τ_{expe} are the calculated and experimental delay-times, respectively, and the maximum error,

$$E_{\text{max}} = \max\left|\frac{\Delta\tau}{\tau_{\text{expe}}}\right|. \tag{3}$$

The absolute values are used to avoid that the positive and negative errors cancel out.

Table 3 shows the mean error for each model and mixture studied. The most accurate model is that of Konnov with a mean error around 20 %. Its predictions are very accurate for all mixtures but mixture 10, C_2H_2–N_2O–O_2–Ar. The GRI-mech 3.0 and the mechanism of Dagaut demonstrate much higher disagreement with the experimental values. The GRI-mech gives satisfactory predictions for mixtures 1–7 but significantly fails in reproducing the experimental delay-times for mixtures 8–10. The mechanism of Dagaut is the best for the mixtures containing methane as the only fuel. Its predictions for the mixtures 4 and 9 are relatively correct. For all the other mixtures, the predictions of Dagaut's mechanism are far from the experimental values. The predictions of the Blanquart mechanism are close to those of the Konnov mechanism as illustrated in Fig. 6. The agreement for all mixtures are satisfactory except for mixture 8, C_2H_4–N_2O–O_2–Ar. Although close to the Konnov mechanism in terms of performance, the Blanquart mechanism demonstrates a smaller maximum error than the Konnov mechanism and overall, it reproduces better the shape of the emission profiles. This feature is illustrated in Fig. 7 for the two acetylene-based mixtures studied. For mixture 9, the OH* profile predicted by the mechanism of Konnov is completely inconsistent with the experimental emission profile. For mixture 10, the pre-ignition emission is largely overestimated by Konnov's mechanism which leads to an inconsistent profile shape. Although the Blanquart mechanism cannot reproduce all the features observed experimentally, it allows to accurately reproduce both the ignition delay-time and the shape of the emission profile. Consequently, it has been used to interpret in more detail the kinetics of the studied mixtures.

3.2.3 Important chemical pathways

To identify the important chemical pathways in both mixtures with and without oxygen, sensitivity and reaction pathway analyses have been performed using Senkin.

Figure 8 presents the normalized sensitivity coefficients with respect to temperature obtained at intermediate temperature for mixtures 3 and 4 and mixtures 7 and 8. In the case of mixtures without oxygen, the two dominant reactions are $N_2O(+M) = N_2 + O(+M)$ and $N_2O + H = N_2 + OH$. The other important reactions all involved consumption or production of the H atom. In the case of mixtures containing both N_2O and O_2, the most important reaction is $H + O_2 = OH + O$. The thermal decomposition of nitrous oxide does not appear within the 10 most sensitive reactions for mixture 4 and is ranked 7th for mixture 8. The sensitivity coefficient of $N_2O + H = N_2 + OH$ is about twice smaller for mixtures with oxygen, about 0.25 compared to about 0.5. The other most sensitive reactions involve consumption and production of H and O atoms.

Figure 9 shows the reaction pathway diagram obtained for mixtures 9 and 10 at T_5 = 1,500 K and P_5 = 300 kPa. For clarity, only 15 species have been included in the diagram. To emphasize the most important pathways, a threshold of 10 % has been applied before calculating the consumption and production percentages. The frames in the diagram represent species reservoirs. To point out the similarities and differences between the kinetics of mixtures 9 and 10, common paths, paths specific to mixture 9 and paths specific to mixture 10 are displayed in different colors. The presence of molecular oxygen in the initial mixture induces a modification of the chemical pathways which involve the very reactive radicals, H, O and OH. In mixture 10, the branching reaction $H + O_2 = OH + O$ accounts for 22 % of H atom consumption and 24 and 40 % of the production of OH and O, respectively. In mixture 9, the reverse reaction $O + OH = H + O_2$ dominates and accounts for 26 % of H atom production and

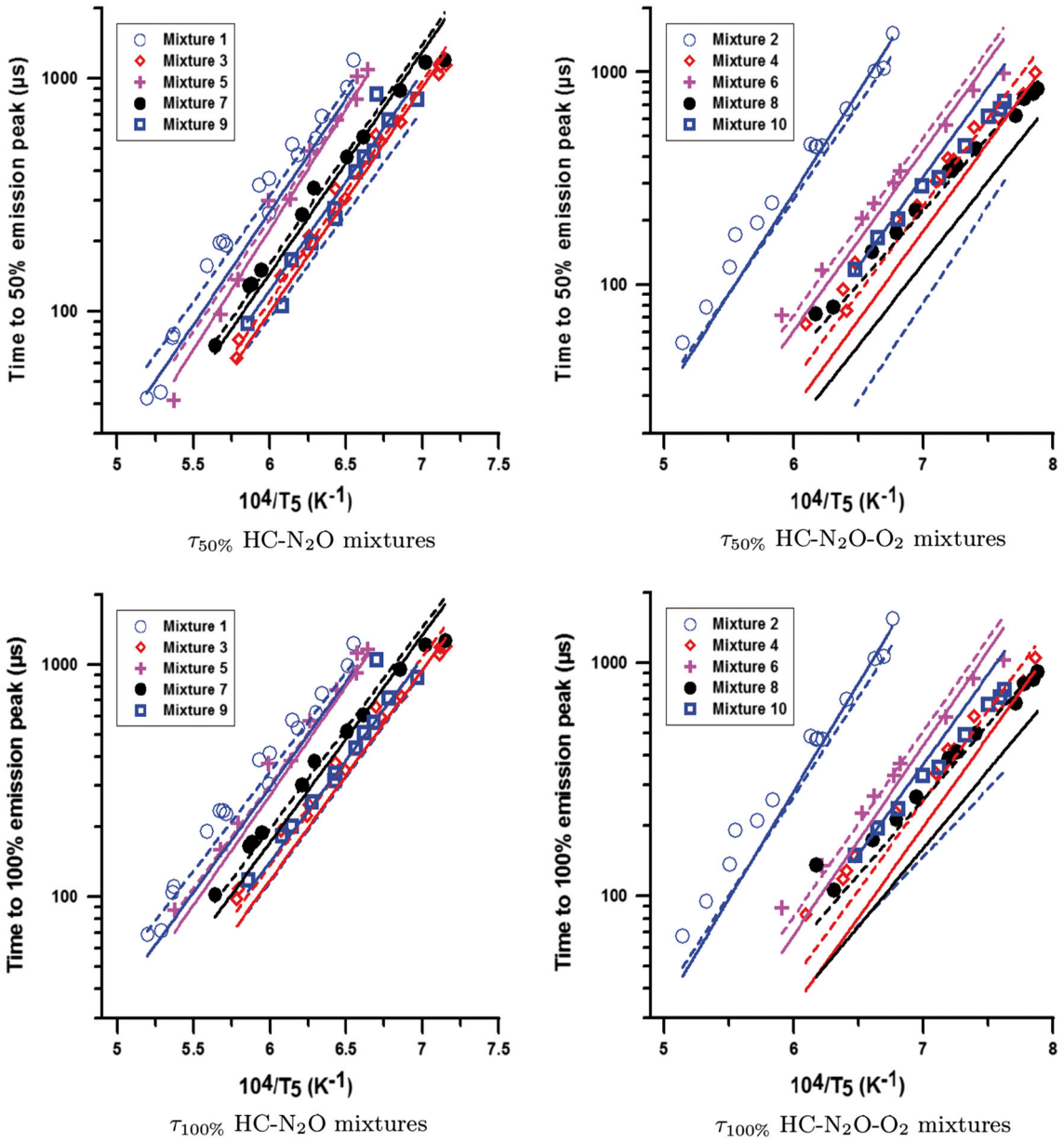

Fig. 6 Comparison between the prediction of the Konnov and Blanquart mechanisms and the experimental delay-times of small hydrocarbons–N_2O(–O_2) mixtures. *Solid lines* Blanquart. *Dashed lines* Konnov

33 and 41 % of the consumption of OH and O, respectively. In mixture 9, OH radicals are formed almost exclusively by $N_2O + H = N_2 + OH$. The importance of the thermal decomposition of N_2O in the formation of O atoms decreases from 100 to 45 % between mixtures 9 and 10. The presence of O_2 also allows for some specific reactions to occur such as $T - CH_2 + O_2 = 2H + CO_2$ or $CH + O_2 = HCO + O$ ($T - CH_2$ stands for the triplet form of the CH_2 radical).

The present results along with previous results obtained for H_2–O_2–N_2O [26,32] and HC-O_2 [33,34] mixtures demonstrate that the addition of nitrous oxide in fuel–O_2 impacts the ignition process chemistry through $N_2O + H = N_2 + OH$. For mixtures which contain only N_2O, the ignition is due to a thermally driven linear chain process which involves $N_2O(+M) = N_2 + O(+M)$ and $N_2O + H = N_2 + OH$ [17], the ignition of mixtures which include O_2 is controlled by the well-known chain branching process. The reaction $N_2O + H = N_2 + OH$ competes with $H + O_2 = OH + O$ for the consumption of H atoms, and contributes to the production of OH radicals. This reaction is exothermic and induces an increase of the mixture temperature and thus the overall reaction rate.

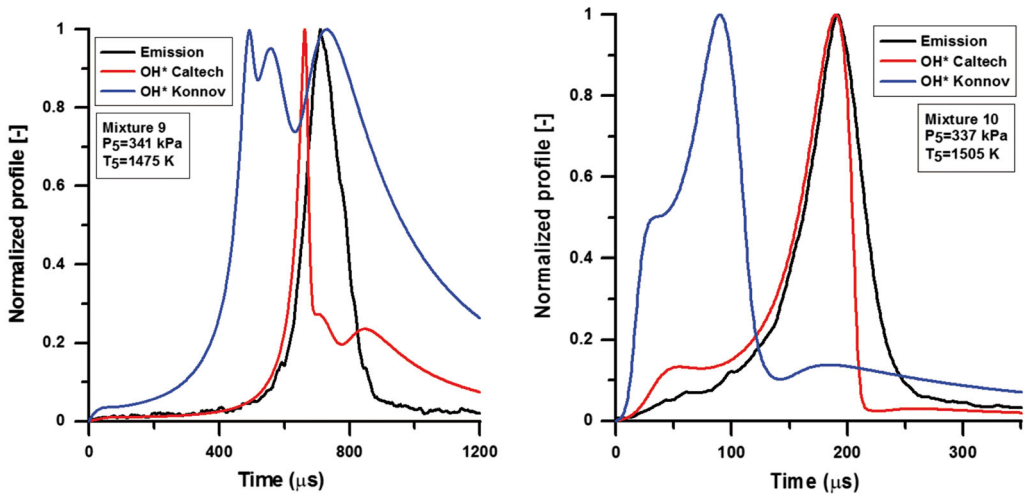

Fig. 7 Experimental normalized emission signals and predicted OH* profiles from Konnov and Blanquart mechanisms

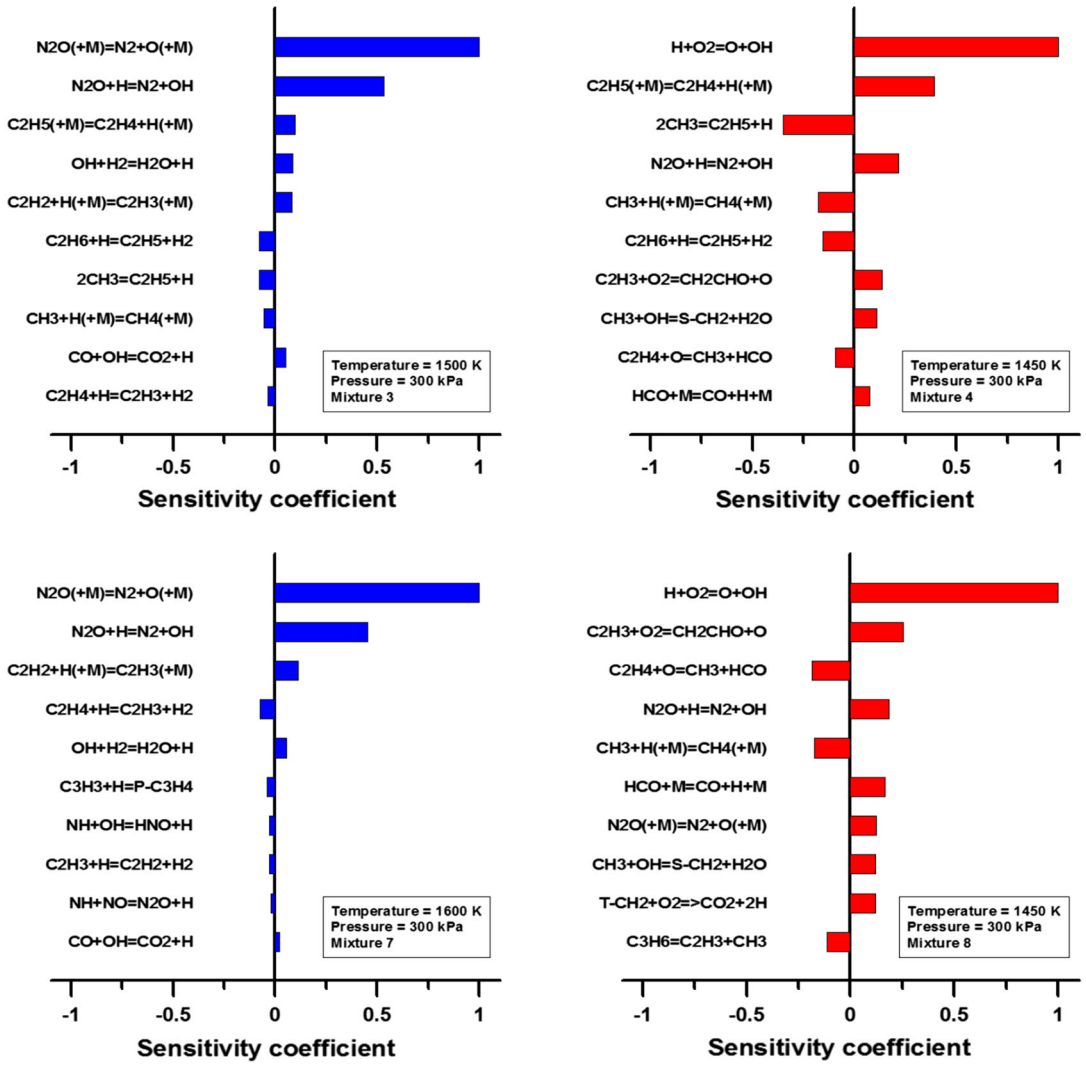

Fig. 8 Normalized sensitivity coefficients with respect to temperature during the oxidation of small hydrocarbon–N_2O(–O_2) mixtures

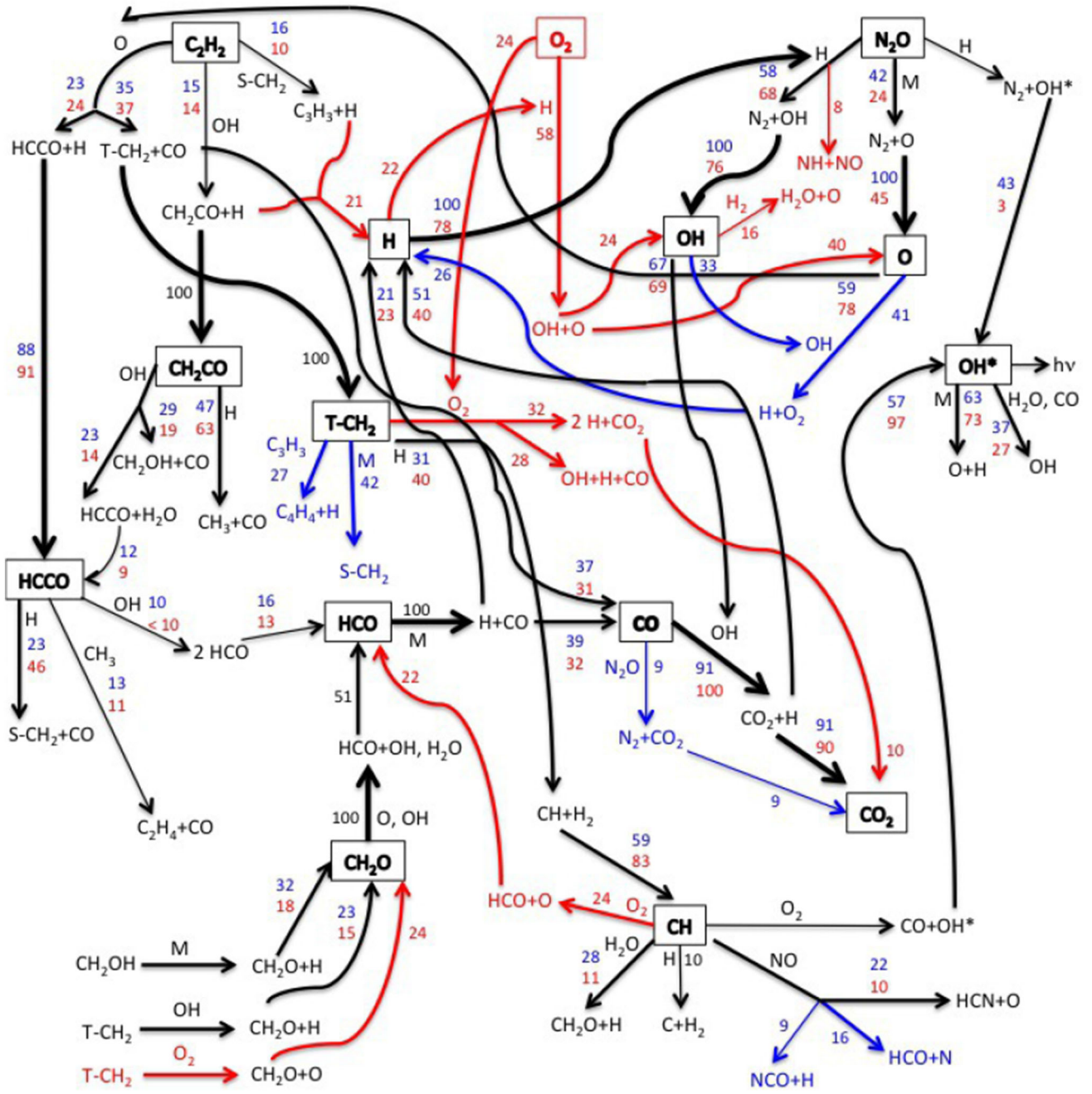

Fig. 9 Reaction pathway diagram of the oxidation of C_2H_2 by N_2O (and O_2). Conditions: $T_5 = 1500$ K and $P_5 = 300$ kPa. The *frames* represent species reservoirs. *Black* common paths; *blue* specific paths for mixture 9; *red* specific paths for mixture 10

3.2.4 Emission feature analysis

Figure 10 compares the experimental OH* emission profiles with the predicted OH* in the case of single-peak profiles. Normalized OH* rates of production (ROP) are also displayed. The analysis of the OH* rates of production shows that for the mixtures containing N_2O only, the formation of OH* is mainly due to R1: $N_2O + H = N_2 + OH^*$, with a smaller contribution of R2: $CH + O_2 = CO + OH^*$. For the mixtures containing both N_2O and O_2, the formation of OH* is exclusively due to R2. For all mixtures, the destruction of OH* is dominated by the reverse of R3: $H + O + M = OH^* + M$.

The energy release dynamics for experiments exhibiting single-peak emission profiles have been studied through temperature derivative and energy release per reaction analysis. Figure 11 presents the results of these analyses for mixtures 1 and 4. In both cases, the energy release is dominated by

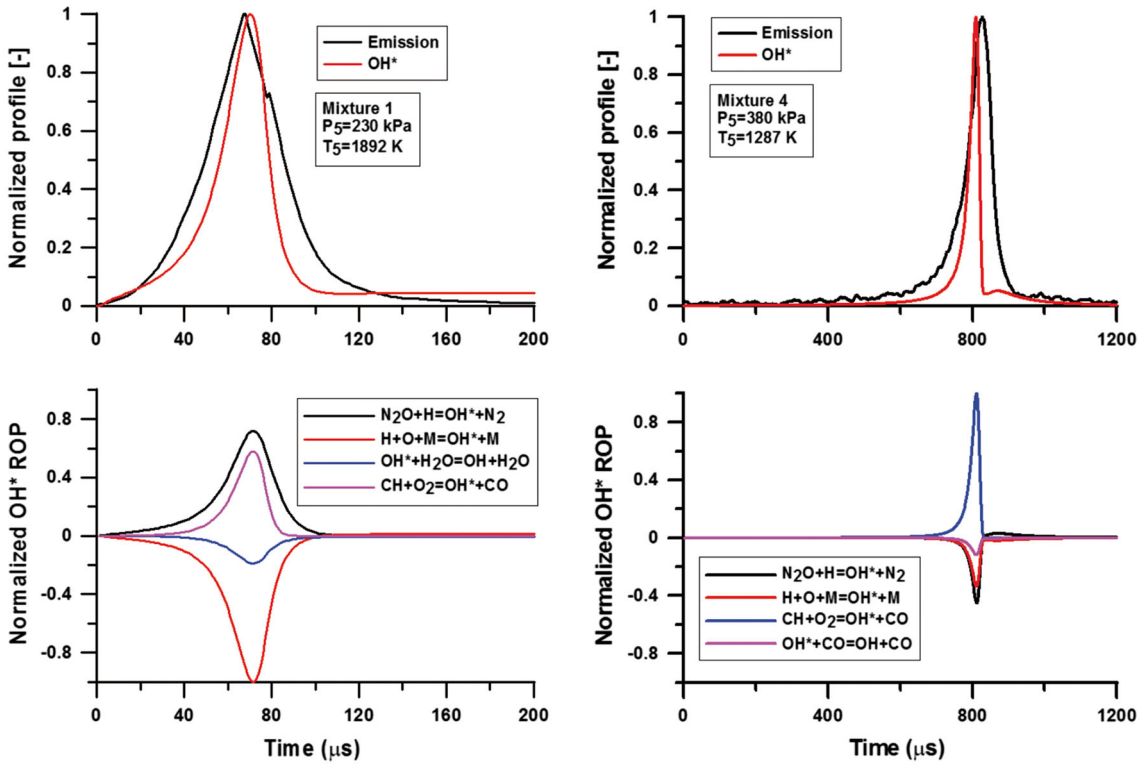

Fig. 10 Experimental emission signals and predicted OH* profiles and ROP for single-peak profiles

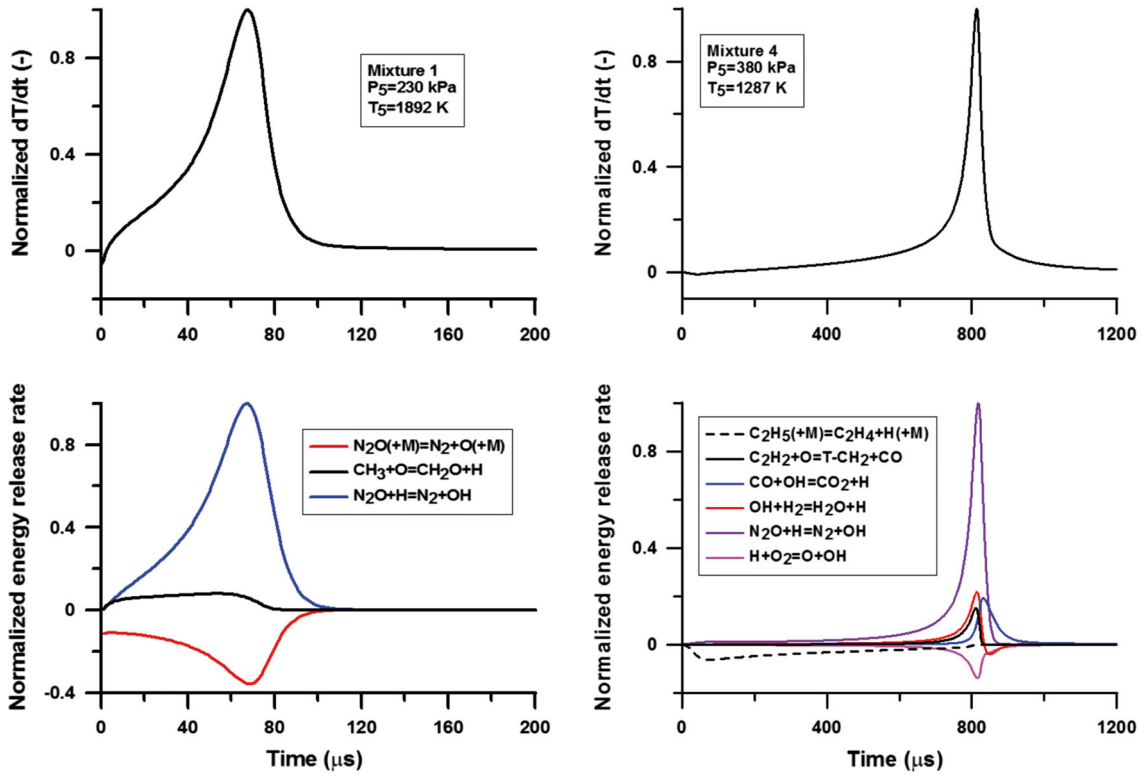

Fig. 11 Temperature derivative profiles and energy release per reaction analysis for experiments with single-peak emission profiles

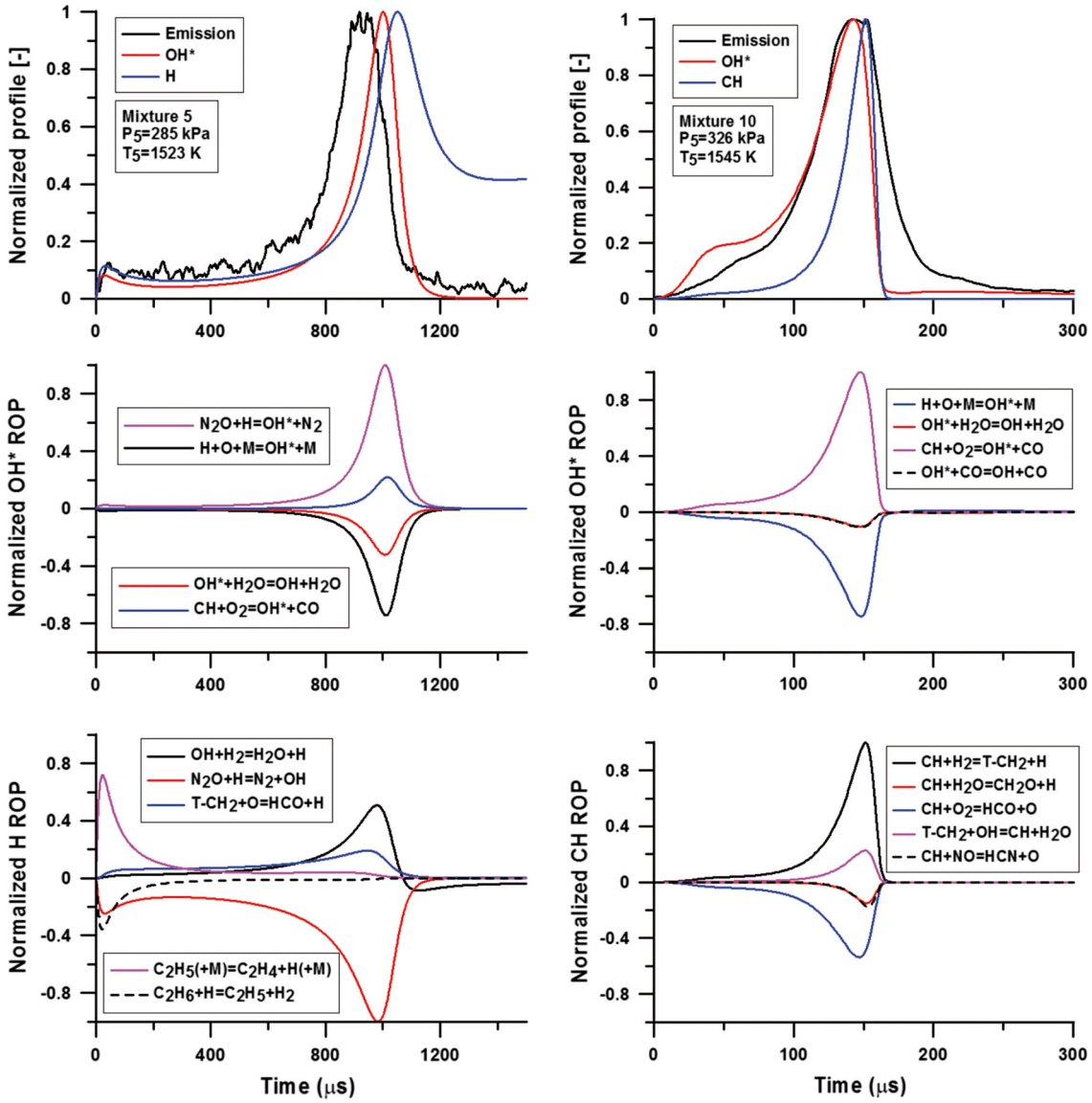

Fig. 12 Experimental emission signals and predicted OH*, H, CH profiles, and H and CH ROP profiles for experiments with pre-ignition emission

the very exothermic reaction R4: $N_2O + H = N_2 + OH$. In the case of mixture 1, which contains only N_2O, the thermal decomposition of nitrous oxide plays a significant role in absorbing heat. The reaction rate of this process increases as the overall reaction proceeds because of the mixture temperature increase. In the case of mixture 4, which contains both N_2O and O_2, the nitrous oxide decomposition is not significant in the energy release. In addition to R4, three other reactions contribute to the temperature increase: R5: $OH + H_2 = H_2O + H$; R6: $CO + OH = CO_2 + H$; and R7: $C_2H_2 + O = T - CH_2 + CO$. At early times, the thermal decomposition of C_2H_5, R8, induces a slight temperature decrease. As the reaction accelerates and increasing amounts of OH radicals are produced, the contribution of the endothermic branching reaction R9: $H + O_2 = O + OH$ in absorbing heat increases.

Results for experiments with pre-ignition emission peaks are illustrated in Fig. 12 which shows typical experimental emission signals along with predicted OH*, H, CH profiles, and H and CH rate of production profiles. The pre-ignition emission peak observed for some of the mixtures can be explained by a two-step production of the main precursors of OH*. For the C_2H_6–N_2O mixtures with and without methane, the main precursor of OH* is the H atom. Initially, the production of H is due to R8: $C_2H_5(+M) = C_2H_4 + H(+M)$. Subsequently, the formation of H is due to R5: $OH + H_2 = H_2O + H$ and R6: $CO + OH = CO_2 + H$. For the mixtures containing C_2H_2 or

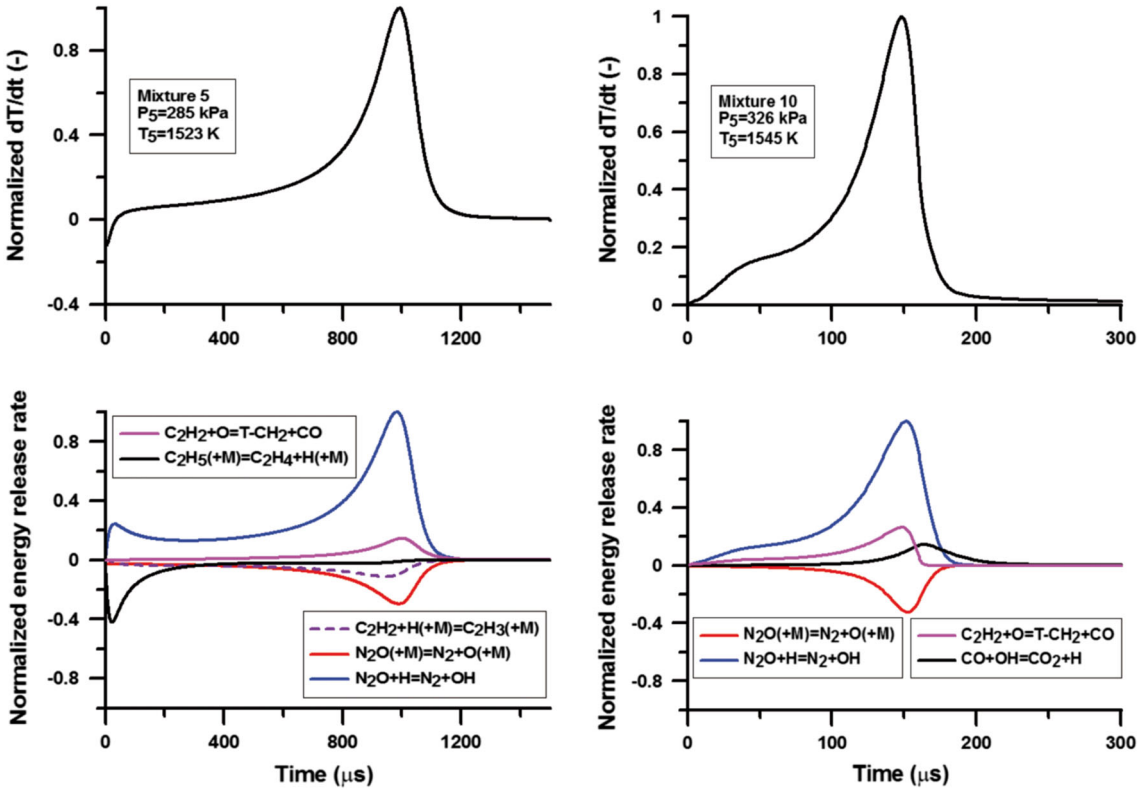

Fig. 13 Temperature derivative profiles and energy release per reaction analysis for experiments with pre-ignition emission

C_2H_4, the main precursor is the CH radical. In both phases, CH is formed by R10: $T - CH_2 + H = CH + H_2$.

Figure 13 shows the temperature derivative and energy release per reaction analysis obtained for experiments with pre-ignition emission. The observation made for experiments with single-peak emission profiles also applies: the energy release in dominated by R4: $N_2O + H = N_2 + OH$. Interestingly, it is seen that for mixture 5, the pre-ignition emission feature is accompanied by a temperature decrease, whereas for mixture 10, there is a temperature increase. The initial endothermic period observed for mixture 5 is due to R8 which is the reaction forming the H atom, the precursor of OH*. The rate of R4 is too low to counter-balance the endothermic decomposition of ethyl radicals. In the case of mixture 10, no endothermic process is significant enough to counter-balance the energy release by R4.

4 Conclusion

In the present study, ignition delay-times of small hydrocarbon–N_2O mixtures with and without O_2 were experimentally measured. The addition of oxygen results in a decrease of the effective activation energy of the oxidation process by 25 % on average. Complex emission profiles have been observed for some of the mixtures. These profiles are characterized by pre-ignition emission peaks. Four detailed reaction models have been evaluated with respect to the present data. The model from Blanquart was able to reproduce satisfactorily both the ignition delay-times and the emission profile shapes. Sensitivity and reaction pathway analyses have demonstrated that the ignition is mostly driven by $N_2O(+M) = N_2 + O(+M)$ and $N_2O + H = N_2 + OH$, for mixtures with only N_2O, and by $N_2O + H = N_2 + OH$ and $H + O_2 = OH + O$ for mixtures which include oxygen. While the reaction rate of $H + O_2$=OH + O is well established that of $N_2O + H = N_2 + OH$ is less so and should be reappraised for improving modeling of nitrous oxide-containing mixtures. In addition, rate constants for hydrocarbon dehydrogenation reactions should be further studied to reduce their uncertainties [35].

Future work will focus on the experimental and modeling study of the high-temperature oxidation of nitro-alkanes and nitrate compounds to develop accurate reaction models for the gas phase kinetics of solid propellants.

Acknowledgments The present work was performed in the Explosion Dynamics Laboratory of the California Institute of Technology. The authors acknowledge the help of Dr P. A. Boettcher, Dr J. Damazo, and A. Demenay for setting up the shock tube. The authors thank Professor G. Blanquart, Caltech, for providing his reaction mechanism and Doctor D. Davidenko for his help with the VTIM code.

References

1. Osmont, A., Catoire, L., Gökalp, I., Yang, V.: Ab initio quantum chemical predictions of enthalpies of formation, heat capacities, and entropies of gas-phase energetic compounds. Combust. Flame **151**, 262–273 (2007)
2. Melius, C., Piqueras, M.: Initial reaction steps in the condensed-phase decomposition of propellants. Proc. Combust. Inst. **29**, 2863–2871 (2002)
3. Toland, A., Simmie, J.: Ignition of alkyl nitrate/oxygen/argon mixtures in shock waves and comparisons with alkanes and amines. Combust. Flame **132**, 556–564 (2003)
4. Presles, H., Desbordes, D., Guirard, M., Guerraud, C.: Gaseous nitromethane and nitromethane-oxygen mixtures: a new detonation structure. Shock Waves **6**, 111–114 (1996)
5. Joubert, F., Desbordes, D., Presles, H.: Detonation cellular structure in NO_2/N_2O_4–fuel gaseous mixtures. Combust. Flame **152**, 482–495 (2008)
6. Joubert, F.: Etude de la détonation de mélanges réactifs gazeux constitués d'un combustible (H_2, CH_4, C_2H_6, C_2H_4) et d'un oxyde d'azote, N_2O et NO_2/N_2O_4. Ph.D. thesis, Université de Poitiers (2001)
7. Parker, W., Wolfhard, H.: Some characteristics of flames supported by NO and NO_2. Symposium (Int.) Combust. **4**, 420–428 (1953)
8. Gray, P., Yoffe, A.D.: The reactivity and structure of nitrogen dioxide. Chem. Rev. **55**, 1069–1154 (1955)
9. Miller, E., Setzer, H.: Burning structure and stability of n-butane-nitrogen dioxide flames in air. Symposium (Int.) Combust. **6**, 164–172 (1957)
10. Allen, M., Yetter, R., Dryer, F.: The decomposition of nitrous oxide at $1.5 < P < 10.5$ atm and $1103 < T < 1173$ K. Int. J. Chem. Kinet. **27**, 883–909 (1995)
11. Javoy, S., Mével, R., Paillard, C.E.: A study of N_2O decomposition rate constant at high temperature: application to the reduction of nitrous oxide by hydrogen. Int. J. Chem. Kinet. **41**, 357–375 (2009)
12. Mével, R.: Etude de mécanismes cinétiques et des propriétés explosives des mélanges hydrogène-protoxyde d'azote et silane-protoxyde d'azote. Application à la sécurité industrielle. Ph.D. thesis, Université d'Orléans (2009)
13. Konnov, A.: Detailed reaction mechanism for small hydrocarbons combustion. Release 0.5 (2000)
14. Le Cong, T.: Etude expérimentale et modélisation de la cinétique de combustion de combustibles gazeux : Méthane, gaz naturel et mélanges contenant de l'hydrogène, du monoxyde de carbone, du dioxyde de carbone et de l'eau. Ph.D. thesis, Université d'Orléans (2007)
15. Smith, G., Golden, D., Frenklach, M., Moriarty, N., Eiteneer, B., Goldenberg, M., Bowman, C., Hanson, R., Song, S., Gardiner, W., Lissianski, V. Qin, Z.: GRI-mech release 3.0
16. Mével, R., Javoy, S., Dupré, G.: A chemical kinetic study of the oxidation of silane by nitrous oxide, nitric oxide and oxygen. Proc. Combust. Inst. **33**, 485–492 (2011)
17. Mével, R., Javoy, S., Lafosse, F., Chaumeix, N., Dupré, G., Paillard, C.E.: Hydrogen-nitrous oxide delay time: shock tube experimental study and kinetic modelling. Proc. Combust. Inst. **32**, 359–366 (2009)
18. Javoy, S., Mével, R., Dupré, G.: Oxygen atom kinetics in silane–hydrogen–nitrous oxide mixtures behind reflected shock waves. Chem. Phys. Lett. **500**, 223–228 (2010)
19. Blanquart, G., Pepiot-Desjardins, P., Pitsch, H.: Chemical mechanism for high temperature combustion of engine relevant fuels with emphasis on soot precursors. Combust. Flame **156**, 588–607 (2009)
20. Hong, Z., Davidson, D., Hanson, R.: An improved H_2/O_2 mechanism based on recent shock tube/laser absorption measurements. Combust. Flame **158**, 633–644 (2011)
21. Hall, J., Rickard, M., Petersen, E.: Comparison of characteristic time diagnostics for ignition and oxidation of fuel/oxidizer mixtures behind reflected shock waves. Combust. Sci. Technol. **177**, 455–483 (2005)
22. Hall, J., Petersen, E.: An optimized kinetics model for OH chemiluminescence at high temperature and atmospheric pressures. Int. J. Chem. Kinet. **38**, 714–724 (2006)
23. Mével, R., Lafosse, F., Catoire, L., Chaumeix, N., Dupré, G., Paillard, C.E.: Induction delay times and detonation cell size prediction of hydrogen–nitrous oxide–argon mixtures. Combust. Sci. Technol. **180**, 1858–1875 (2008)
24. Hall, J., Reehal, S., Petersen, E.: Kinetics of the OH chemiluminescence in the presence of silicon. Chem. Phys. Lett. **425**, 229–233 (2006)
25. Pichon, S.: Etude cinétique de systèmes hypergoliques et propergoliques à base d'éthanol et de peroxide d'hydrogène. Ph.D. thesis, Université d'Orléans (2005)
26. Mevel, R., Pichon, S., Catoire, L., Chaumeix, N., Paillard, C.E., Shepherd, J.E.: Dynamics of excited hydroxyl radicals in hydrogen-based mixtures behind reflected shock waves. Proc. Combust. Inst. **34**, 677–684 (2013)
27. Lutz, A., Kee, R., Miller, A.: SENKIN : a fortran program for predicting homogeneous gas phase chemical kinetics with sensitivity analysis. Technical report Sand87-8248, Sandia International Laboratories (1992)
28. Kee, R., Grcar, J., Smooke, M., Miller, J.: A fortran program for modelling steady laminar one-dimensional premixed flames. Technical report SAND85-8240, Sandia International Laboratories (1993)
29. Chaos, M., Dryer, F.: Chemical-kinetic modeling of ignition delay: considerations in interpreting shock tube data. Int. J. Chem. Kinet. **42**, 143–150 (2010)
30. Rotavera, B., Dagaut, P., Petersen, E.: Chemical kinetics modeling of n-nonane oxidation in oxygen/argon using excited-state species time histories. Combust. Flame **161**, 1146–1163 (2014)
31. Damazo, J., Ziegler, J., Karnesky, J., Shepherd, J.E.: Shock wave-boundary layer interaction from reflecting detonations. In: Proceedings of the 28th International Symposium on Shock Waves, vol 2, pp. 751–756 (2012)
32. Mathieu, O., Levacque, A., Petersen, E.: Effects of N_2O addition on the ignition of H_2–O_2 mixtures: experimental and detailed kinetic modeling study. Int. J. Hydrogen Energy **37**, 15393–15405 (2012)
33. Mével, R., Javoy, S., Coudoro, K., Dupré, G., Paillard, C.E.: Assessment of H_2–CH_4–air mixtures oxidation kinetic models used in combustion. Int. J. Hydrogen Energy **37**, 698–714 (2012)
34. Glassman, I.: Combustion. Academic Press Inc., London (1987)
35. Baulch, D.L., Bowman, C.T., Cobos, C.J., Cox, R.A., Just, T., Kerr, J.A., Pilling, M.J., Stocker, D., Troe, J., Tsang, W., Walker, R.W., Warnatz, J.: Evaluated kinetic data for combustion modeling: supplement II. J. Phys. Chem. Ref. Data **34**, 757–1397 (2005)